International Journal of Steel Structures 18(1): 13-23 (2018)
DOI 10.1007/s13296-018-0302-9
ISSN 1598-2351 (Print)
ISSN 2093-6311 (Online)

International Journal of
STEEL
STRUCTURES
www.springer.com/journal/13296

A Study of Different Microstructural Effects on the Strain Hardening Behavior of Hadfield Steel

Burak Bal*

Department of Mechanical Engineering, Abdullah Gül University, 38080, Kayseri, Turkey

Abstract

The effects of the initial texture, velocity gradient, strain increment and type of interaction tensor on the strain hardening response of Hadfield steel were investigated. To observe their influences on mechanical response, crystal plasticity computations were carried out with the aid of the Visco-Plastic Self-Consistent (VPSC) algorithm. Specifically, uniaxial deformation response of Hadfield steel was modeled based on the experimental deformation response at a strain rate of 1×10^{-1} s^{-1} and corresponding Voce hardening parameters were calculated. The same Voce hardening parameters were utilized with different boundary conditions in the VPSC simulations to identify the roles of the aforementioned microstructural properties. The current results demonstrate the importance of these microstructural properties for reliable predictions of the strain hardening response of Hadfield steel and constitute an important guideline for the proper selection of them.

Keywords: hadfield steel, crystal plasticity, VPSC, polycrystal, mechanical behavior, modeling

1. Introduction

High-manganese austenitic steels (HMnAS) provide a great potential in several areas, such as automotive, railway and construction industries, owing to the unique combination of high strength and sustained ductility they offer (Adler *et al*., 1986; Bal *et al*., 2015; Dastur and Leslie, 1981). The resulting high work hardening, high energy absorption capacity, and their superior resistance to impact wear have already made them the materials of choice in various applications (Canadinc, 2005; Frommeyer *et al*., 2003; Grassel *et al*., 2000). The high work hardening capacity of HMnAS results from the coexistence of diverse micro-mechanisms, including dislocation slip (Karaman *et al*., 2001b, 2000b), twinning (Gumus *et al*., 2016; Karaman *et al*., 2001a, 2001b, 2000b), and phase transformation (Wen *et al*., 2014). In addition to these primary mechanisms of plastic deformation, additional microstructural features, such as interactions of these primary mechanisms (Canadinc *et al*., 2007b, 2005; Gumus *et al*., 2016; Karaman *et al*., 2000b), stacking faults (Efstathiou and Sehitoglu, 2010; Shtremel and Kovalenko, 1987), dynamic strain aging (DSA) (Bal *et al*., 2016; Owen and Grujicic, 1999), and alloying elements (Gumus *et al*., 2015; Owen and Grujicic, 1999; Raghavan *et al*., 1969) have been shown to significantly contribute to the exceptional work hardening capacity of this class of steels. All these mechanisms act as potential obstacles against dislocation motion (Hutchinson and Ridley, 2006; Karaman *et al*., 2000b).

Stacking fault energy (SFE), which is mainly dictated by temperature and alloying elements, is the key factor for the activation of the aforementioned mechanisms (Allain *et al*., 2004; Shen *et al*., 2013). Specifically, as the temperature increases, the Gibbs free energy change needed for deformation also increases, which results in higher SFE values (Bouaziz *et al*., 2011; Curtze and Kuokkala, 2010). On the contrary, alloying elements display individual effects on SFE. For instance, even though the addition of Al increases the SFE, addition of Si decreases it.

One of the very good examples of high-manganese austenitic steels with complicated microstructure is Hadfield steel with 1.2-1.4 wt% C and 12-14 wt% Mn (Feng *et al*., 2013). The crystal lattice structure of Hadfield steel is face-centered cubic (FCC) at room temperature. Hadfield steel possesses a higher stacking fault energy ~50 mJ/m^2 (SFE) compared to twinning induced plasticity (TWIP~25 mJ/m^2) steel and transformation induced plasticity (TRIP~20 mJ/m^2) steel (Allain *et al*., 2004; Bal *et al*., 2015; Gumus *et al*., 2015; Kang *et al*., 2014). If the SFE level is less than 35 mJ/m^2, it is easier to pass the energy barriers to accommodate abrupt changes

Received August 4, 2016; accepted April 12, 2017;
published online March 31, 2018

*Corresponding author
Tel: +90 352 224 8800, Fax: +90 352 338 8828
E-mail: burak.bal@agu.edu.tr

which enhances twin formation. However, when the SFE level is higher than 35 mJ/m^2, slip becomes the favorable deformation mechanism during plastic deformation (Kibey *et al*., 2007). Thereby, Hadfield steel is mainly deformed by both twinning and slip. During the deformation, the interactions of these mechanisms increase the strain hardening response of Hadfield steel. In addition, due to DSA, caused by the reorientation of carbon members of C-Mn clusters in the dislocation core, Hadfield steel exhibits heterogeneous plastic deformation by repeated nucleation and propagation of shear bands and negative strain rate sensitivity (Anjabin *et al*., 2013; Canadinc *et al*., 2008). More specifically, carbon atoms block dislocation glide when they meet dislocations, which is known as pinning of dislocations, and cause serrations in the strain hardening response of Hadfield steel. These instabilities in the material response have been known as jerky flow or Portevin-Le Chatelier (PLC) effect (Fressengeas *et al*., 2005). The PLC effect in metallic materials has been investigated by several researchers utilizing acoustic emission, digital image correlation (DIC), laser scanning extensometry techniques but reliable results could not be observed due to experimental problems such as signals arising from the acoustic emission source, dependence of DIC results to sample surface preparation and inability of obtaining unidimensional information in laser extensometry (Chmelík *et al*., 2007; Renard *et al*., 2010; Wang *et al*., 2007; Yilmaz, 2011). Therefore, different modeling efforts have been carried out to observe the PLC effect together with experimental analyses and the success in these simulations, from atomic scale to mesoscale, has provided more comprehensive information about the complicated strain hardening response of materials in association with microstructural events.

The complicated microstructure of Hadfield steel and associated superior mechanical properties have been subject to various experimental observations and modeling efforts. Experimental studies were conducted utilizing different types of tests such as tensile (Canadinc *et al*., 2008), compressive (Feng *et al*., 2013), fatigue (Kang *et al*., 2014), and impact (Bal *et al*., 2015) loadings together with microstructural observations with the aid of scanning electron microscopy, transmission electron microscopy and confocal microscopy. In the modeling part, the effect of twinning on strain hardening response of Hadfield steel was studied (Karaman *et al*., 2000a). Also, the effects of dislocation sheet structures (Canadinc *et al*., 2005), grain boundary misorientation angle (Canadinc *et al*., 2011), high density dislocation walls (HDDWs) (Canadinc *et al*., 2007a), slip-twin interactions (Canadinc *et al*., 2007b) and DSA (Bal *et al*., 2016) were incorporated into crystal plasticity computations. After incorporating DSA into crystal plasticity, corresponding negative strain rate sensitivity of Hadfield steel was also captured. In addition, the Bauschinger effect was studied (Karaman *et al*., 2001b), the model, which incorporates the pile-up stresses, SFE and friction stress, was suggested to predict the orientation and stress direction effects in the critical resolved shear stress for twinning (Karaman *et al*., 2000b). All of the aforementioned crystal plasticity computation efforts were carried out using the Visco-Plastic Self-Consistent (VPSC) algorithm. However, all of these works were carried out under certain conditions such as specific initial texture, velocity gradient, strain increment and type of interaction tensor, and neither of them have so far presented the effect of these circumstances on the strain hardening response of Hadfield steel.

The current study was undertaken with the intention of elucidating the effects of the aforementioned parameters on the strain hardening response of Hadfield steel. In particular, deformation response of Hadfield steel was modeled at a strain rate of 1×10^{-1} s^{-1}. Using the same hardening mechanism and different interaction choices such as, n^{eff}=10, tangent, Taylor and Relative directional compliance criterion (RDC), for the linear behavior at the grain level, the effects of these approaches on the macroscopic deformation behavior of the Hadfield steel were monitored. In addition, different velocity gradient tensors, different strain increments and different textures with the same hardening parameters were tried for the same purpose. The current findings from the following study demonstrate that the selection of the aforementioned input parameters is very important for crystal plasticity modeling. Furthermore, the effect of each input for the VPSC modeling are defined clearly. Overall, the current results shed light on the role of each individual studied input on the strain hardening mechanism of Hadfield steel.

2. Experimental Observations and Mechanism

In a previous study (Canadinc *et al*., 2008), tensile tests were conducted for the Hadfield steel specimens with a chemical composition of 12.44 wt. % Mn, 1.10 wt. % C and balance Fe, at strain rates from 1×10^{-1} s^{-1} to 1×10^{-4} s^{-1} at ambient temperature,. Initial samples possessed a random texture. Details of the experiments can be found from the author's previous work (Bal *et al*., 2016). With the aid of microstructural observations through scanning electron microscopy (SEM) and transmission electron microscopy (TEM), the strain hardening mechanisms of the Hadfield steel were identified as the combination of slip, twinning, DSA, HDDWs and dislocation-grain boundary interactions. Subsequently, these mechanisms were modeled successfully at the slip system scale using VPSC (Bal *et al*., 2016; Canadinc *et al*., 2011, 2005). The remaining question here, however, is how sensitive this modeling tool is to different inputs, which is answered in the following section.

3. Theory and Calculations

During the original set of crystal plasticity simulations, texture and crystal structure, experimentally measured as random and FCC respectively, and number of grains of the material were utilized as a direct input and 12 primary slip systems were activated to model the material response of Hadfield steel. For a system (s), the corresponding resolved shear stress (τ^s_{RSS}) driving plastic deformation is defined in terms of the vector forms of the Schmid tensor (m^s_i) and the applied stress (σ_i) as:

$$\tau^s_{RSS} = m^s_i \sigma_i \tag{1}$$

The nonlinear shear strain rate in the system s can be described as a function of τ^s_{RSS}:

$$\dot{\gamma}^s = \dot{\gamma}_0 \left(\frac{\tau^s_{RSS}}{\tau^s_0} \right)^n = \dot{\gamma}_0 \left(\frac{m^s_i \sigma_i}{\tau^s_0} \right)^n \tag{2}$$

where $\dot{\gamma}_0$ is a reference rate, τ^s_0 is the threshold stress corresponding to this reference rate, and n is the inverse of the rate sensitivity index. The superposition of the contributions from all active systems gives the total strain rate in a crystal, which can be presented in its pseudo-linearized form as in the following expression (Lebensohn and Tomé, 1993):

$$\dot{\varepsilon}_i = \left[\dot{\gamma}_0 \sum_1^s \frac{m^s_i m^s_j}{\tau^s_0} \left(\frac{m^s_k \sigma_k}{\tau^s_0} \right)^{n-1} \right] \sigma_j = \tilde{M}^{c(\sec)}_{ij}(\tilde{\sigma}) \sigma_j \tag{3}$$

where $\tilde{M}^{c(\sec)}_{ij}$ is the secant visco-plastic compliance of the crystal which gives the instantaneous relation between stress and strain rate. At the polycrystal level, this relationship assumes the following form (Lebensohn and Tomé, 1993):

$$\dot{E}_i = M^{(\sec)}_{ij}(\tilde{\Sigma}) \Sigma_j + \dot{\Sigma}^0 \tag{4}$$

where $\dot{E}_i$ and $\dot{\Sigma}$ represent the polycrystal strain rate and applied stress, respectively.

In a continuum that consists of a matrix and inclusions, the deviations in strain rate and stress between the inclusion and their overall magnitudes are defined as:

$$\tilde{\dot{\varepsilon}}_k = \dot{\varepsilon}_k - \dot{E}_k \tag{5}$$

$$\tilde{\sigma}_j = \sigma_j - \Sigma_j \tag{6}$$

where $\dot{\varepsilon}_k$ and σ_j stand for the local (single crystal or grain level) strain rate and stress. Utilizing Eshelby's inhomogeneous inclusion formulation one can solve the stress equilibrium equation to derive (Kocks *et al*., 1998):

$$\tilde{\dot{\varepsilon}} = -\tilde{M} : \tilde{\sigma} \tag{7}$$

There are different linearization methods available in VPSC, namely, secant, tangent, n^{eff}=10, taylor and RDC.

Secant linearization schema is defined as:

$$M^{(\sec)}_{ijkl} = \gamma_0 \Sigma_s \frac{m^s_{ij} m^s_{kl}}{\tau^s} \left(\frac{m^s : \sigma}{\tau^s} \right)^{n-1} \tag{8}$$

where $M^{(\sec)}$ is the secant compliance tensor for the polycrystal aggregate. Tangent linearization schema and secant linearization schema are proportional to each other such that (Hutchinson, 1976):

$$M^{(\tan)} = n M^{(\sec)} \tag{9}$$

Even though the tangent and secant linearization schemas assume that the same compliance captures the local response of modeled material, tangent method provides more homogenous local stress distribution within the matrix (Lebensohn and Tomé, 1993). Other linearization schemas are suggested for introducing an adjustable parameter n^{eff}:

$$\tilde{M}^c = n^{\text{eff}} (I - S)^{-1} : S : M^{(\sec)} \tag{10}$$

where S is the visco-plastic Eshelby tensor (Kocks *et al*., 1998) and n^{eff} represents the strength of the coupling between the stress deviations and the strain rate deviations. For Taylor interaction n^{eff}=0, for secant interaction n^{eff}=1 and for RDC interaction n^{eff}=1< n^c < n.

Since the original simulations were conducted with secant linearization, the interaction tensor $\tilde{M}$ is defined as:

$$\tilde{M} = n' (I - S)^{-1} : S : M^{(\sec)} \tag{11}$$

Substitution of Eqs. 3 and 4 into Eq. 7 yields the macroscopic secant compliance, $M^{(\sec)}$, and the macroscopic strain rate is evaluated by taking the weighted average of crystal strain rates over all the grains as in Eq. 12:

$$M^{(\sec)} = \langle M^{c(\sec)} : (M^{c(\sec)} + \tilde{M})^{-1} : (M^{(\sec)} + \tilde{M}) \rangle \tag{12}$$

Iterative solution of the Eqs. 3, 7 and 12 gives the stress in each grain, the crystal's compliance tensor, and the polycrystal compliance consistent with the applied strain rate E_i. In all sets of simulations, the term n in Eq. 2 was chosen as 20, which makes the formulation rate insensitive (Lebensohn and Tomé, 1993). As for the interaction in Eq. 11, an effective value of n' =1 was used in all original simulations, which ensures a rigid interaction (Lebensohn and Tomé, 1993).

The rate of overall dislocation density can be expressed as:

$$\dot{\rho} = \Sigma_n \{ k_1 \sqrt{\rho} - k_2 \rho \} \left| \dot{\gamma}^n \right| \tag{13}$$

where k_1 and k_2 are constants that define the athermal (statistical) storage of the moving dislocations and dynamic recovery in the domains outside the HDDWs, respectively (Canadinc *et al*., 2003).

The flow stress τ is defined in the traditional Taylor hardening format as:

$$\tau - \tau_0 = \alpha\mu b\sqrt{\rho} \tag{14}$$

After taking the time derivative of the flow stress with constant reference strength, the rate of the flow stress is obtained as:

$$\dot{\tau} = \frac{\alpha\mu b\dot{\rho}}{2\sqrt{\rho}} \tag{15}$$

Substituting Eq. 13 into Eq. 15 results in:

$$\dot{\tau} = \Sigma_n\left[\left\{k_1\frac{\alpha\mu b}{2} - k_2\frac{\alpha\mu b\sqrt{\rho}}{2}\right\}\left|\dot{\gamma}^n\right|\right] \tag{16}$$

From Eq. 14, the following identity is obtained for the square root of the density of dislocations:

$$\sqrt{\rho} = \frac{\tau - \tau_0}{\alpha\mu b} \tag{17}$$

Once Eq. 17 is substituted into Eq. 16, the rate of flow stress evolution is given by:

$$\dot{\tau} = \Sigma_n\left[\left\{k_1\frac{\alpha\mu b}{2} - k_2\frac{\tau - \tau_0}{2}\right\}\left|\dot{\gamma}^n\right|\right] \tag{18}$$

One should note that the term $\left\{k_1\frac{\alpha\mu b}{2} - k_2\frac{\tau - \tau_0}{2}\right\}$ in Eq. 18 is the linear Voce hardening term (Eq. 20). Having noted this, Eq. 18 can also be written as:

$$\dot{\tau} = \Sigma_n\left[\left\{\theta_0\left(\frac{\tau_s - \tau}{\tau_s - \tau_0}\right)\right\}\left|\dot{\gamma}^n\right|\right] \tag{19}$$

where θ_0 is the constant strain hardening rate, and τ_s represents the saturation stress in the absence of geometric effects, or the threshold stress. The hardening is defined by an extended Voce law (Kocks *et al*., 1998), which is characterized by the evolution of the threshold stress (τ^s) with accumulated shear strain (Γ) in each grain of the form:

$$\tau^s = \tau_0 + (\tau_1 + \theta_1\Gamma)\left(1 - \exp\left(-\frac{\theta_0\Gamma}{\tau_1}\right)\right) \tag{20}$$

where τ_0 is the reference strength, and τ_1, θ_0 and θ_1 are the parameters that define the hardening behavior (Kocks *et al*., 1998). The hardening law defined by Eq. 20 characterizes the onset of plasticity and the saturation of threshold stress at larger strains.

The classical Voce hardening scheme in Eq. 19 was modified to incorporate the effects of DSA, HDDWs, dislocation-grain boundary interactions according to Eqs. 21, 22 and 23 respectively (Bal *et al*., 2016; Canadinc *et al*., 2011, 2005):

$$\dot{\tau} = \Sigma_n\left[\left\{\theta_0\left(\frac{\tau_s - \tau}{\tau_s - \tau_0}\right)\right\}\left|\dot{\gamma}^n\right| + M_i S\frac{d\tau_{CD}}{dt}\right] \tag{21}$$

$$\dot{\tau} = \Sigma_n\left[\left\{\theta_0\left(\frac{\tau_s - \tau}{\tau_s - \tau_0}\right)\right\} + \frac{K\alpha^2\mu^2 b}{4t(\tau - \tau_0)}\Sigma_r\cos\theta_{nr}\right]\left|\dot{\gamma}^n\right| \tag{22}$$

$$\dot{\tau} = \Sigma_n\left[\left\{\theta_0\left(\frac{\tau_s - \tau}{\tau_s - \tau_0}\right)\right\} + \frac{K\alpha^2\mu^2 b}{2d(\tau - \tau_0)}\Sigma_q(1 + \sin\theta_q)\right]\left|\dot{\gamma}^n\right| \tag{23}$$

where M_i is the instantaneous strain rate sensitivity, S is the scaling factor that reflects the contribution of carbon to the overall hardening response throughout the whole grain, τ_{CD} is the shear stress due to solute carbon atom, K is the geometric constant and the terms $\Sigma_n\Sigma_r\frac{K}{cb}\cos\theta_{nr}\left|\dot{\gamma}^n\right|$ and $\Sigma_n\Sigma_q\frac{K}{db}(1 + \sin\theta_q)\left|\dot{\gamma}^n\right|$ account for the contribution due to the interaction between the dislocations on the active slip system n and the active twin system r and the interaction between the dislocations on the active slip system n and the boundary between the grain in consideration and its q^{th} neighbor, respectively (Biyikli *et al*., 2010; Canadinc *et al*., 2011, 2007a, 2005). The angle θ_{nr} is the angle between the plane normal of active slip system and the plane normal of active twinning system, and was incorporated to measure the role of slip-twin interactions in a geometric sense. Moreover, the angle θ_q is the misorientation angle between the surface normals of neighboring grains.

For all the simulations average grain shape is assumed for each grain when calculating the Eshelby tensor. Also, initial ellipsoid ratios describing average grain shape were 1.0, 1.0, 1.0. The relative tolerance allowed in the convergence procedures was 0.02. The maximum number of iterations used for the convergence of the external loop was 200 and the internal loop was 20. The number of points used for the Gaussian integration of Eshelby tensor was inputted as 24 since the grains are not highly distorted and it is sufficient enough to preserve the precision of the integration (Lebensohn and Tomé, 1993).

4. Results and Discussion

Figure 1 shows the true stress-true strain (SS) curves of the Hadfield steel at room temperature until 0.18 true strain. The serrations in the SS curves arise from DSA (Bal *et al*., 2016; Koyama *et al*., 2013, 2011; Lee *et al*., 2011). Specifically, as the strain rate increases, the energy

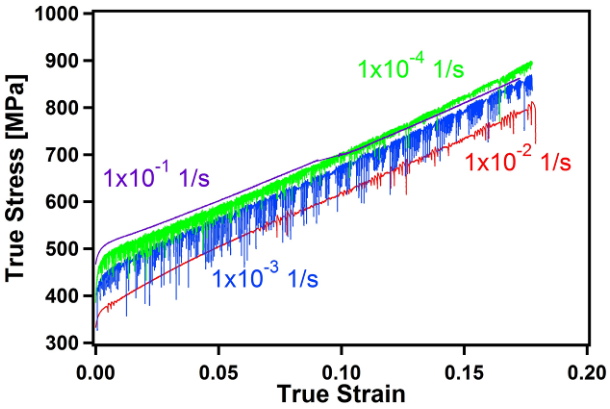

Figure 1. The room temperature uniaxial tensile deformation response of HS obtained at different strain rates. The data were recompiled from (Canadinc *et al*., 2008).

of the specimen also increases, which triggers the diffusivity of carbon. When solute carbon diffuses more in the host matrix, the probability of dislocation pinning by carbon reduces, which decreases the contribution of DSA on strain hardening, and corresponding negative strain rate sensitivity (NSRS) is observed (Fig. 1). However, at the highest strain rate, DSA becomes negligible when compared to excessive forest hardening, therefore at very high strain rates strain hardening response of the Hadfield steel is mainly dictated by forest hardening instead of DSA, which results in positive strain rate sensitivity (Canadinc *et al*., 2008). There are two dominant primary hardening mechanisms for Hadfield steel. These are DSA, due to reorientations of carbon members of Mn-C clusters in the dislocation core, and forest hardening. For low strain rates, DSA is the primary cause of rapid strain hardening due to the fact that more time is provided for dislocation-C interactions which promote DSA (Canadinc, 2005; Dastur and Leslie, 1981). Therefore as the strain rate increases from 1×10^{-4} s^{-1} to 1×10^{-2} s^{-1}, the effect of DSA decreases and the effect of forest dislocations on hardening do not change considerably and low stress values at the same strain values are observed. However, once the strain rate increases from 1×10^{-2} s^{-1} to 1×10^{-1} s^{-1}, the effect of forest dislocations increases dramatically while the effect of DSA on hardening response decreases. That is why the lowest yield point was observed for the 1×10^{-2} s^{-1} strain rate case.

Figure 2 shows the set of crystal plasticity modeling results of the uniaxial deformation response of Hadfield steel at strain rates ranging from 1×10^{-1} s^{-1} to 1×10^{-4} s^{-1}. Classical Voce hardening law was used (Eq. 20) and corresponding hardening parameters are given in Table 1. The serrations in the deformation response were captured using Eq. 21, which incorporates DSA into VPSC computations in the previous study (Bal *et al*., 2016). Modeling effort was carried out neglecting the elastic deformation response of Hadfield steel since VPSC is

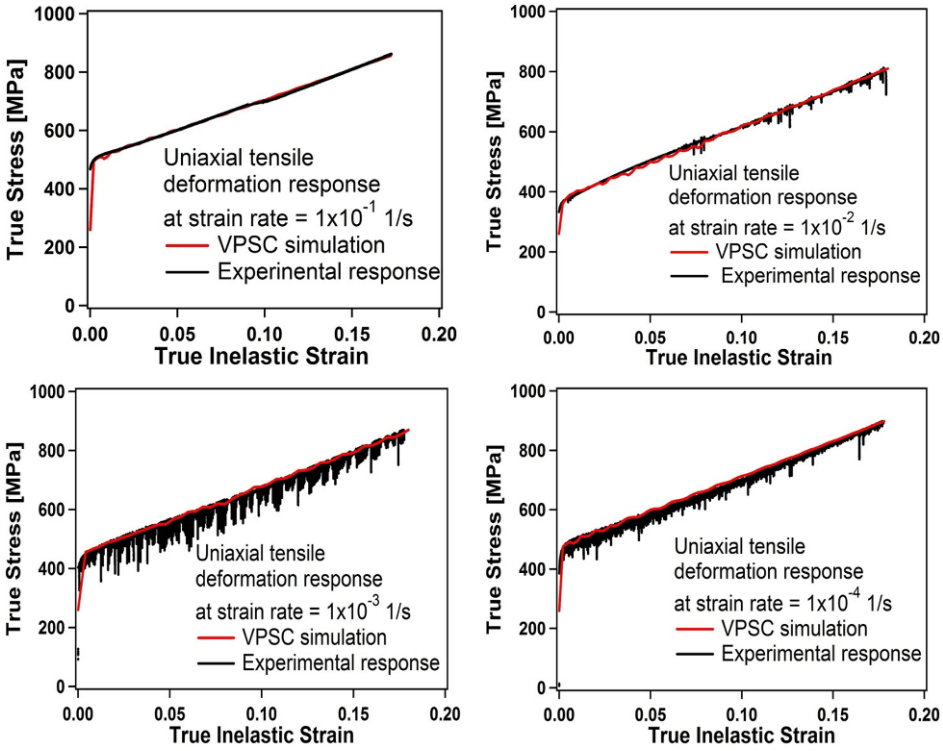

Figure 2. VPSC simulations of the room temperature experimental uniaxial tensile deformation of Hadfield steel at different strain rates. The data were recompiled from (Bal *et al.*, 2016).

Table 1. Voce hardening parameters utilized in VPSC simulations for each strain rate

Strain rate (s^{-1})	τ_0 (MPa)	τ_1 (MPa)	θ_0 (MPa)	θ_1 (MPa)
1×10^{-1}	132	925	53×10^{4}	350
1×10^{-2}	132	147	43×10^{3}	408
1×10^{-3}	132	1580	60×10^{4}	390
1×10^{-4}	132	918	55×10^{4}	398

capable of modeling only plastic behavior of materials until necking. It has been demonstrated that proper modeling at the slip system level enables to achieve macroscopic material response of materials (Canadinc *et al*., 2005; Karaman *et al*., 2000a). Therefore, proper adjustment of the boundary conditions and the input parameters is of the utmost importance in any crystal plasticity model. The novelty of the following results is the identification of the effects of different linearization schemas, velocity gradients, strain increments and textures on the microscale based deformation response of Hadfield steel. Even though Hadfield steel was selected as the studied material since its microstructure is complicated, such that, simultaneous activity of different micro-deformation mechanism, which are slip, twin, stacking faults, DSA and their interactions, dictates the deformation response of Hadfield steel and author has previous experience on Hadfield steel both experimentally (Bal *et al*., 2015) and theoretically (Bal *et al*., 2016), the results of this study will be applicable to all metallic materials. Original simulations were conducted considering primary {111}<110> slip with 12 systems, random texture, secant type of inclusion-matrix interaction and a strain increment of 0.00173 per step, and corresponding Voce hardening parameters were computed. τ_0, which is the microyield strength or critical resolved shear stress, was calculated as 132 MPa. The same Voce hardening parameters were utilized in all other sensitivity analysis simulations in order to follow the same hardening trend and to observe the role of each individual parameter on the overall hardening response of Hadfield steel at room temperature.

Figure 3 shows the dependence of strain hardening response of Hadfield steel on the linearization method used during the simulation. The strain hardening response of Hadfield steel during deformation up to 0.18 strain was modeled successfully by using secant interaction. The initial modeling result is in good agreement with the nature of the dislocation theory (Hirth, JP Lothe, 1968), which states that secant linearization schema is a stiff method, hence more stable results can be obtained using this method. Using tangent and n^{eff}=10 interactions causes serrations at each strain increment and thus they do not provide a steady-state hardening response (Fig. 3). Changing linearization schema from secant to tangent, RDC and n^{eff}=10 increases the stress level at the same strain up to 0.1 strain, unlike previously reported studies, which state that the effective compliance of the matrix increases as the parameter n^{eff} increases (Karaman *et al*., 2000a; Onal *et al*., 2014). After 0.1 strain, RDC and n^{eff}=10 interactions tend to provide more consonant response with secant interaction. Unlike other interactions, using Taylor model causes a decrease in the stress values up to 0.1 strain, which then provides consistent results with secant interaction. Only the RDC linearization schema assumes that the interaction strength between grain and matrix is different for each grain, whereas others assume it is the same for all grains. Current results agree well with the findings of the previous work (Tome, 1999).

Figure 4 shows the dependence of strain hardening response of Hadfield steel on the velocity gradient, which is the sum of all crystallographic slip rates on the active slip systems, used during the simulation. Accurate determination of the velocity gradient tensor is crucial for the modeling of deformation behavior of polycrystalline aggregates. Velocity gradient tensor could be calculated directly from the deformation history (Onal *et al*., 2015), crystal plasticity calculations (Koester *et al*., 2012; Patra

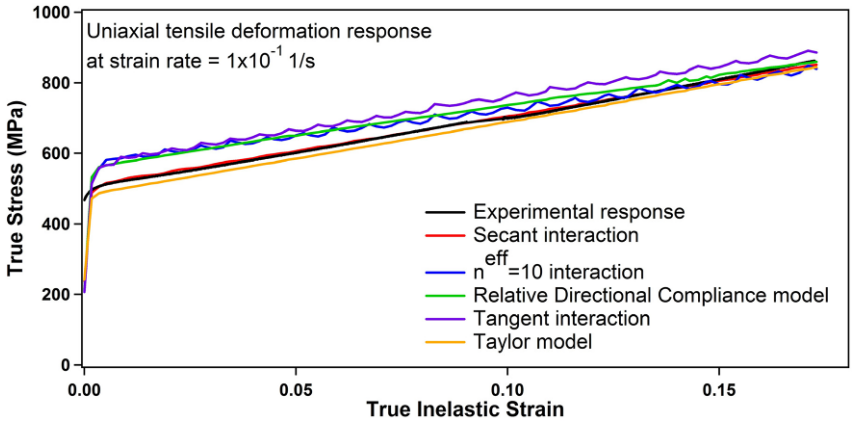

Figure 3. VPSC simulations of the room temperature experimental uniaxial tensile deformation of Hadfield steel with different linearization methods at a strain rate of 1×10^{-1} s^{-1}.

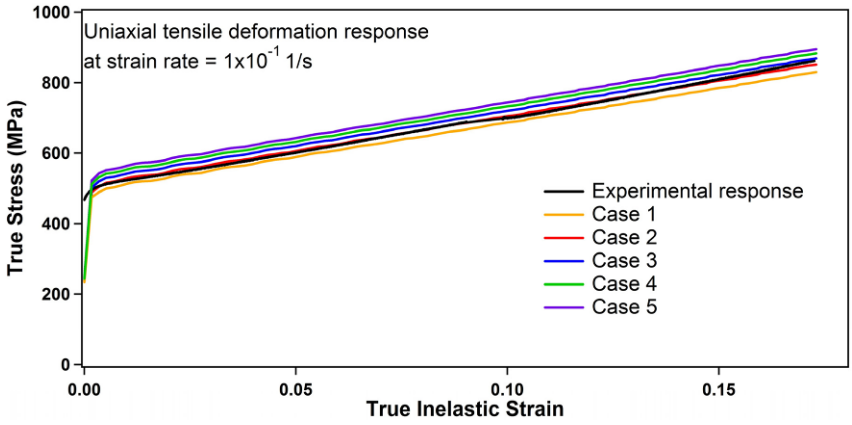

Figure 4. VPSC simulations of the room temperature experimental uniaxial tensile deformation of Hadfield steel with different velocity gradients at a strain rate of 1×10^{-1} s^{-1}.

Table 2. Employed velocity gradient in during the simulations for each case

	L_{11}	L_{22}	L_{33}	L_{12}	L_{13}	L_{21}	L_{23}	L_{31}	L_{32}
Case 1	1	-0.05	-0.95	0	0	0	0	0	0
Case 2	1	-0.075	-0.925	0	0	0	0	0	0
Case 3	1	-0.1	-0.90	0	0	0	0	0	0
Case 4	1	-0.125	-0.875	0	0	0	0	0	0
Case 5	1	-0.15	-0.85	0	0	0	0	0	0

et al., 2014), finite element frame (Mirzajanzadeh and Canadinc, 2016) or based on normal and shear stress distributions (Onal *et al*., 2014) depending on the loading scenarios. The list of velocity gradient tensor components for each case employed in the current study was tabulated in Table 2. Since uniaxial loading was given as a boundary condition during simulations, symmetric components of the velocity gradient tensors were set to zero. The summation of the diagonal components of the velocity gradient tensor was chosen as zero for crystal plasticity computations. It should be noted that the strength levels attained from crystal plasticity computations is linearly proportional to L_{22}. Specifically, as the values of L_{22} and L_{33} approach each other, the homogeneity of the deformation increases. The linear proportionality of stress levels to the L_{22} component of the velocity gradient tensor was also observed in previous studies (O. Onal *et al*., 2014; Onal *et al*., 2014).

Figure 5 shows the dependence of strain hardening response of Hadfield steel on the input texture used during the simulation. It is assumed in most of the crystal plasticity modeling studies that initially the material possesses a random texture or the orientation distribution does not show any significant texture; hence random texture was used as an input (Luo *et al*., 2010). However, material may possess a different distribution of crystallographic orientations, or in other words, a preferred orientation rather than random texture. The critical resolved shear stress, necessary to initiate slip in a grain, is calculated based on a Taylor factor through Taylor law and used in Eq. 20 (Stoller and Zinkle, 2000). VPSC computations were carried out with different textures whose Taylor factor values were 3.01, 3.04, 3.06 (random texture) and 3.09. Bishop-Hill method was used for the calculation of Taylor factor. In particular, the orientations of the crystal were transformed into crystal coordinates. Then the work increments for each discrete stress states (vertex) were calculated. Finally, corresponding Taylor factors were computed by dividing the maximum work increment by the von Mises equivalent strain. All of the 28 vertexes that operate slip systems were used for the calculation procedure of Taylor factors. It has been observed that changing input texture has no significant effect on strain hardening response of Hadfield steel at both low strain and moderate strain values, unlike previously reported studies, which state that in polycrystalline materials, plastic anisotropy due to inhomogeneous texture has a significant effect on the macroscopic mechanical behavior, which requires further treatment (Adler *et al*., 1986; Canadinc *et al*., 2007b; Li *et al*., 2013; Mirzajanzadeh and Canadinc, 2016). It has been observed that for the simulations, which were carried out with near to random texture (Taylor factor=3.06), there is not much change in the Taylor factors from initial states of the deformation to fracture. Whereas, once the texture moves away from the random texture, a larger change in the Taylor factor was observed (from 3.01 to 2.98).

Figure 6 shows the dependence of strain hardening response of Hadfield steel on the strain increment used during the simulation. During all crystal plasticity simulations,

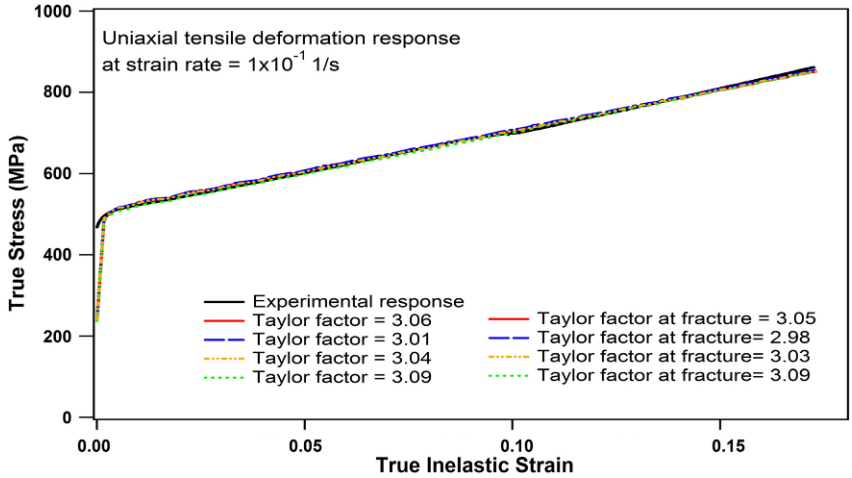

Figure 5. VPSC simulations of the room temperature experimental uniaxial tensile deformation of Hadfield steel with different initial textures at a strain rate of 1×10^{-1} s^{-1}.

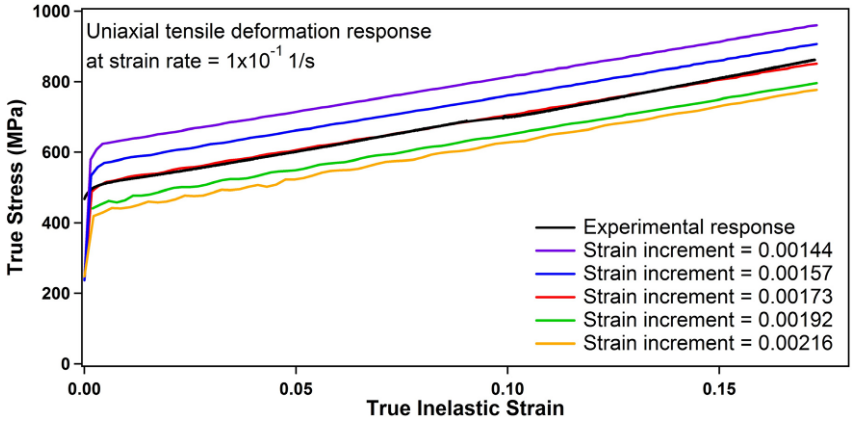

Figure 6. VPSC simulations of the room temperature experimental uniaxial tensile deformation of Hadfield steel with different strain increments at a strain rate of 1×10^{-1} s^{-1}.

Taylor condition of equal strain increment was imposed to every grain. Both strain increment and number of steps designate the final inelastic strain of the simulation, hence proper alignment of strain increment has significant impact on the computational time. As the strain increment increases, crystal plasticity computations were carried out with less number of steps which decreases both the accuracy of results and computational time. However, one may want to assess the success of a desired model also at large strain increments. For instance, observing serration due to a solute carbon atom at large strain increments or effects of high dense dislocation walls at large strain increments. The main objective should be decreasing the computation time without sacrificing from accuracy. As the strain increment decreases using the same hardening rule, the stress-strain curve becomes smoother, whereas at higher strain increments the fluctuations in the material response are visible, which demonstrates that increasing strain increment deteriorates the material response (Fig. 6). In order to eliminate this drawback, unique hardening models were proposed to predict the contributions of DSA and corresponding NRSS, HDDWs and slip-twin interactions on the strain hardening of Hadfield steel at large strain increments without deteriorating the material response (Bal *et al*., 2016; Canadinc *et al*., 2007a, 2007b). Furthermore, stress values are inversely proportional to strain increment, or in other words, as the strain increment increases attained stress values at the same strain levels decreases (Fig. 6). The current results show that increasing strain increment without changing the hardening rule decreases the accuracy of results and determination of the contributions of different hardening mechanisms on the overall material response at large strain increments can be achieved by incorporating new hardening models.

5. Conclusion

In this study, the effects of initial texture, velocity gradient, strain increment and type of interaction tensor on the material response of Hadfield steel were investigated by crystal plasticity computations. For this purpose,

uniaxial tensile deformation response of Hadfield steel at room temperature and at a strain rate of 1×10^{-1} s^{-1} was modeled and corresponding Voce hardening parameters were calculated. In order to identify the roles of the aforementioned microstructural properties, VPSC simulations were carried out with the same hardening parameters but different boundary conditions. The simulation results demonstrate that stress levels at the same strain levels are linearly proportional to the L_{22} component of the velocity gradient tensor and inversely proportional to strain increment. Furthermore, even though the linearization method used during the simulation has a significant effect on the material response of Hadfield steel, no dramatic effect of texture on the material response of Hadfield steel was observed. Consequently, the current findings shed light on the effects of each individually studied input on the strain hardening mechanism of Hadfield steel and constitute a step forward and an important guideline for the proper selection of different microstructural properties.

References

Adler, P.H., Olson, G.B., and Owen, W.S. (1986). "Strain Hardening of Hadfield Manganese Steel." *Metallurgical Transactions A,* 17, pp. 1725-1737.

Allain, S., Chateau, J.-P., Bouaziz, O., Migot, S., and Guelton, N. (2004). "Correlations between the Calculated Stacking Fault Energy and the Plasticity Mechanisms in Fe-Mn-C Alloys." *Materials Science and Engineering: A,* 387-389, pp. 158-162.

Anjabin, N., Karimi Taheri, A., and Kim, H.S. (2013). "Simulation and Experimental Analyses of Dynamic Strain Aging of a Supersaturated Age Hardenable Aluminum Alloy." *Materials Science and Engineering: A,* 585, pp. 165-173.

Bal, B., Gumus, B., and Canadinc, D. (2016). "Incorporation of Dynamic Strain Aging into a Visco-Plastic Self-Consistent Model for Predicting the Negative Strain Rate Sensitivity of Hadfield Steel." *Journal of Engineering Materials and Technology,* 138, pp. 1-8.

Bal, B., Gumus, B., Gerstein, G., Canadinc, D., and Maier, H.J. (2015). "On the Micro-Deformation Mechanisms Active in High-Manganese Austenitic Steels under Impact Loading." *Materials Science and Engineering A,* 632, pp. 29-34.

Biyikli, E., Canadinc, D., Maier, H.J., and Niendorf, T., Top, S. (2010). "Three-Dimensional Modeling of the Grain Boundary Misorientation Angle Distribution Based on Two-Dimensional Experimental Texture Measurements." *Materials Science and Engineering A,* 527, pp. 5604-5612.

Bouaziz, O., Allain, S., Scott, C.P., Cugy, P., and Barbier, D. (2011). "High Manganese Austenitic Twinning Induced Plasticity Steels: A Review of the Microstructure Properties Relationships." *Current Opinion in Solid State and Materials Science,* 15, pp. 141-168.

Canadinc, D. (2005). PhD Thesis. University of Illinois at Urbana-Champaign, USA.

Canadinc, D., Biyikli, E., Niendorf, T., and Maier, H.J. (2011). "Experimental and Numerical Investigation of the Role of Grain Boundary Misorientation Angle on the Dislocation-Grain Boundary Interactions." *Advanced Engineering Materials,* 13, pp. 281-287.

Canadinc, D., Efstathiou, C., and Sehitoglu, H. (2008). "On the Negative Strain Rate Sensitivity of Hadfield Steel.", *Scripta Materialia* 59, pp. 1103-1106.

Canadinc, D., Karaman, I., Sehitoglu, H., Chumlyakov, Y.I., and Maier, H.J. (2003). "The Role of Nitrogen on the Deformation Response of Hadfield Steel Single Crystals." *Metallurgical and Materials Transactions A,* 34, pp. 1821-1831.

Canadinc, D., Sehitoglu, H., and Maier, H.J. (2007a). "The Role of Dense Dislocation Walls on the Deformation Response of Aluminum Alloyed Hadfield Steel Polycrystals." *Materials Science and Engineering: A,* 454-455, pp. 662-666.

Canadinc, D., Sehitoglu, H., Maier, H.J., and Chumlyakov, Y.I. (2005). "Strain Hardening Behavior of Aluminum Alloyed Hadfield Steel Single Crystals." *Acta Materialia,* 53, pp. 1831-1842.

Canadinc, D., Sehitoglu, H., Maier, H.J., Niklasch, D., and Chumlyakov, Y.I. (2007b). "Orientation Evolution in Hadfield Steel Single Crystals under Combined Slip and Twinning." *International Journal of Solids and Structures,* 44, pp. 34-50.

Chmelík, F., Klose, F.B., Dierke, H., Šachl, J., Neuhäuser, and H., Lukáč, P. (2007). "Investigating the Portevin-Le Châtelier Effect in Strain Rate and Stress Rate Controlled Tests by the Acoustic Emission and Laser Extensometry Techniques." *Materials Science and Engineering A,* 462, pp. 53-60.

Curtze, S., and Kuokkala, V. (2010). "Dependence of Tensile Deformation Behavior of TWIP Steels on Stacking Fault Energy, Temperature and Strain Rate." *Acta Materialia,* 58, pp. 5129-5141.

Dastur, Y.N., and Leslie, W.C. (1981). "Mechanism of Work Hardening in Hadfield Manganese Steel." *Metallurgical Transactions A,* 12, pp. 749-759.

Efstathiou, C., and Sehitoglu, H. (2010). "Strain Hardening and Heterogeneous Deformation during Twinning in Hadfield Steel." *Acta Materialia,* 58, pp. 1479-1488.

Feng, X.Y., Zhang, F.C., Yang, Z.N., and Zhang, M. (2013). "Wear Behaviour of Nanocrystallised Hadfield Steel." *Wear,* 305, pp. 299-304.

Fressengeas, C., Beaudoin, A.J., Lebyodkin, M., Kubin, L.P., and Estrin, Y. (2005). "Dynamic Strain Aging: A Coupled dislocation-Solute Dynamic Model." *Materials Science and Engineering: A,* 400-401, pp. 226-230.

Frommeyer, G., Brüx, U., and Neumann, P. (2003). "Supra-Ductile and High-Strength Manganese-TRIP/TWIP Steels for High Energy Absorption Purposes." *ISIJ International,* 43, pp. 438-446.

Grassel, O., Kruger, L., Frommeyer, G., and Meyer, L.W. (2000). "High Strength Fe-Mn-(Al, Si) TRIP/TWIP Steels Development-Properties-Application." *International Journal of Plasticity,* 16, pp. 1391-1409.

Gumus, B., Bal, B., Gerstein, G., Canadinc, D., and Maier, H.J. (2016). "Twinning Activity in High-Manganese

Austenitic Steels under High Velocity Loading." *Materials Science and Technology,* 32, pp. 463-465.

Gumus, B., Bal, B., Gerstein, G., Canadinc, D., Maier, H.J., Guner, F., and Elmadagli, M. (2015). "Twinning Activity in High-Manganese Austenitic Steels under High Velocity Loading." *Materials Science and Engineering A,* 648, pp. 104-112.

Hirth, JP Lothe, J. (1968). "Theory of Dislocations." *McGraw-Hill, New York*: 247..

Hutchinson, B., and Ridley, N. (2006). "On Dislocation Accumulation and Work Hardening in Hadfield Steel." *Scripta Materialia,* 55, pp. 299-302.

Hutchinson, J.W. (1976). "Bounds and Self-Consistent Estimates for Creep of Polycrystalline Materials." *Proceedings of the Physical Society of London A,* 348, pp. 101-121.

Kang, J., Zhang, F.C., Long, X.Y., and Lv, B. (2014). "Cyclic Deformation and Fatigue Behaviors of Hadfield Manganese Steel." *Materials Science and Engineering: A,* 591, pp. 59-68.

Karaman, I., Sehitoglu, H., Beaudoin, A.J., Chumlyakov, Y.I., Maier, H.J., and Tome, C.N. (2000a). "Modeling the Deformation Behavior of Hadfield Steel Single and Polycrystals due to Twinning and Slip." *Acta Materialia,* 48, pp. 2031-2047.

Karaman, I., Sehitoglu, H., Chumlyakov, Y.., Maier, H.., and Kireeva, I.V. (2001a). "Extrinsic Stacking Faults and Twinning in Hadfield Manganese Steel Single Crystals." *Scripta Materialia,* 44, pp. 337-343.

Karaman, I., Sehitoglu, H., Chumlyakov, Y.., Maier, and H.J., Kireeva, I.V. (2001b). "The Effect of Twinning and Slip on the Bauschinger Effect of Hadfield Steel Single Crystals." *Metallurgical and Materials Transactions A,* 32, pp. 695-706.

Karaman, I., Sehitoglu, H., Gall, K., Chumlyakov, Y.I., and Maier, H.J. (2000b). "Deformation of Single Crystal Hadfield Steel by Twinning and Slip." *Acta Materialia,* 48, pp. 1345-1359.

Kibey, S., Liu, J.B., Johnson, D.D., and Sehitoglu, H. (2007). "Predicting Twinning Stress in Fcc Metals: Linking Twin-Energy Pathways to Twin Nucleation." *Acta Materialia,* 55, pp. 6843-6851.

Kocks, U.F., Tomé, C.N., and Wenk, H.R. (1998). "Texture and Anisotropy." *Cambridge University Press: New York*.

Koester, A., Ma, A., and Hartmaier, A. (2012). "Atomistically Informed Crystal Plasticity Model for Body-Centered Cubic Iron." *Acta Materialia,* 60, pp. 3894-3901. doi:10.1016/j.actamat.2012.03.053

Koyama, M., Sawaguchi, T., Lee, T., Lee, C.S., and Tsuzaki, K. (2011). "Work Hardening Associated with ε-Martensitic Transformation, Deformation Twinning and Dynamic Strain Aging in Fe-17Mn-0.6C and Fe-17Mn-0.8C TWIP Steels." *Materials Science and Engineering A,* 528, pp. 7310-7316.

Koyama, M., Sawaguchi, T., and Tsuzaki, K. (2013). "TWIP Effect and Plastic Instability Condition in an Fe-Mn-C Austenitic Steel." *ISIJ International,* 53, pp. 323-329.

Lebensohn, R.A., and Tomé, C.N. (1993). "A Self-Consistent Anisotropic Approach for the Simulation of Plastic Deformation and Texture Development of Polycrystals: Application to Zirconium Alloys." *Acta Metallurgica et Materialia,* 41, pp. 2611.

Lee, S.-J., Kim, J., Kane, S.N., and Cooman, B.C. De (2011). "On the Origin of Dynamic Strain Aging in Twinning-Induced Plasticity Steels." *Acta Materialia,* 59, pp. 6809-6819.

Li, Y., Zhu, L., Liu, Y., Wei, Y., Wu, Y., Tang, D., and Mi, Z. (2013). "On the Strain Hardening and Texture Evolution in High Manganese Steels: Experiments and Numerical Investigation." *Journal of the Mechanics and Physics of Solids,* 61, pp. 2588-2604.

Luo, J., Li, M., Li, X., and Shi, Y. (2010). "Constitutive Model for High Temperature Deformation of Titanium Alloys Using Internal State Variables." *Mechanics of Materials,* 42, pp. 157-165.

Mirzajanzadeh, M., and Canadinc, D. (2016). "A Microstructure-Sensitive Model for Simulating the Impact Response of an High-Manganese Austenitic Steel." *Journal of Engineering Materials and Technology, In Press*

Onal, O., Bal, B., Toker,S.M., Mirzajanzadeh, M., Canadinc, D., and Maier,H.J. (2014). "Microstructure-Based Modeling of the Impact Response of a Biomedical Niobium-Zirconium Alloy." *Journal of Materials Research,* 29, pp. 1123-1134.

Onal, O., Bal, B., Canadinc, D., and Akdari, E. (2015). "Experimental and Numerical Evaluation of Thickness Reduction in Steel Plate Heat Exchangers." *Journal of Engineering Materials and Technology*, 137, pp. 041001-041008

Onal, O., Ozmenci, C., and Canadinc, D. (2014). "Multi-Scale Modeling of the Impact Response of a Strain-Rate Sensitive High-Manganese Austenitic Steel." *Frontiers in Materials,* 1, pp. 1-12.

Owen, W.S., and Grujicic, M. (1999). "Strain Aging of Austenitic Hadfield Manganese Steel." *Acta Materialia,* 47, pp. 111-126.

Patra, A., Zhu, T., and McDowell, D.L. (2014). "Constitutive Equations for Modeling Non-Schmid Effects in Single Crystal Bcc-Fe at Low and Ambient Temperatures." *International Journal of Plasticity,* 59, pp. 1-14.

Raghavan, K.S., Sastri, A.S., and Marcinkowski, M.J. (1969). "Nature of the Work-Hardening Behavior in Hadfield's Manganese Steel." *Transactions of the Metallurgical Society of AIME.,* 245, pp. 1569-1575.

Renard, K., Ryelandt, S., and Jacques, P.J. (2010). "Characterisation of the Portevin-Le Châtelier Effect Affecting an Austenitic TWIP Steel Based on Digital Image Correlation." *Materials Science and Engineering: A,* 527, pp. 2969-2977.

Shen, Y.F., Qiu, C.H., Wang, L., Sun, X., Zhao, X.M., and Zuo, L. (2013). "Effects of Cold Rolling on Microstructure and Mechanical Properties of Fe-30Mn-3Si-4Al-0.093C TWIP Steel." *Materials Science and Engineering: A,* 561, pp. 329-337.

Shtremel, M.A., and Kovalenko, I.A. (1987). "On the Work Hardening Mechanism of Hadfield Steel." *The Physics of Metals and Metallography,* 63, pp. 158-166.

Stoller, R.E., and Zinkle, S.J. (2000). "On the Relationship between Uniaxial Yield Strength and Resolved Shear

Stress in Polycrystalline Materials." *Journal of Nuclear Materials,* 283-287, pp. 349-352.

Tome, C.N. (1999). "Self-Consistent Polycrystal Models: A Directional Compliance Criterion to Describe Grain Interactions." *Modellıng And Sımulatıon In Materıals Scıence And Engıneerıng,* 7, pp. 723-738.

Wang, C., Li, Z., Xu, Y., and Han, E. (2007). "Acoustic Emission Inspection of Portevin-Le Chatelier Effect and Deformation Mechanisms of Two Mg-Li-Al Alloys." *Journal of Materials Science,* 42, pp. 3573-3579.

Wen, Y.H., Peng, H.B., Si, H.T., Xiong, R.L., and Raabe, D. (2014). "A Novel High Manganese Austenitic Steel with Higher Work Hardening Capacity and Much Lower Impact Deformation than Hadfield Manganese Steel." *Materials and Design,* 55, pp. 798-804.

Yilmaz, A. (2011). "The Portevin-Le Chatelier Effect: A Review of Experimental Findings." *Science and Technology of Advanced Materials,* 12, pp. 063001.